Internal Mechanics of Anti Stick-Slip Tool

Mohammad Khodadadi Dehkordi[a], Amin Taraghi Osguei[b,*], Iman Khamoushi[b], Ekaterina Pavlovskaia[a], Marian Wiercigroch[a]

[a] *Centre for Applied Dynamics Research, School of Engineering, University of Aberdeen, Aberdeen AB24 3UE, UK*
[b] *Department of Mechanical Engineering, Sahand University of Technology, Tabriz, Iran*

Abstract

An anti stick-slip tool (ASST) is a mechanical device comprised of two parts connected to each other by a pre-loaded spring and a helical spline, which mathematically is a constraint. This constraint converts an excessive external torque to an axial displacement during operation of the tool, which shortens a drill-string and prevents a drill-bit to get stuck. In this study, a mathematical model of the ASST has been developed for the first time by considering internal friction on the helical spline and a pre-load of the internal spring, where we propose four distinct states of the coupled rotational and axial movements of this tool. The system is described by a non-smooth oscillator when the tool is activated, and by a kinematic relation when the tool is not activated. During operation, axial and rotational movements are applied at the top part of the ASST, and the axial force and torque acting at the bottom are prescribed as external excitations. Parametric studies are presented, and undertaken modelling and the obtained results are first steps to fully understand the mechanics of the ASST, where there is an interplay between the dry friction and the pre-load. This study should help to understand intricacies of the ASST operation, and it can be used to create a more realistic model by relaxing simplifying assumptions to describe the operation of the tool with more fidelity.

Keywords: Drill-string dynamics, stick-slip, anti stick-slip tool, torsional and axial vibrations, dry friction

*Corresponding author.
Email address: taraghi@sut.ac.ir (Amin Taraghi Osguei)

Nomenclature

α	Constraint constant	L	Lead of the thread or helical spline
δ_{P}	Static deflection of spring	l_{t}	Length of thread
μ	Friction coefficient	M_{b}	Mass of BHA below ASST
ϕ_{μ}	Angle of Friction coefficient	N_{R}	Normal force
Φ_{t}	Rotation of ASST at top section	P	Static pre-load force
Φ_{b}	Rotation of ASST at top section	R	Resultant force on threads of helical spline
D_{b}	ASST axial damping coefficient	r_{i}	Effective radius of internal constraint
F_{A}	Internal force without weight of ASST	r_{s}	Mean radius of helical spline
F_{a}	Activation force	T_{a}	Activation torque
F_{e}	External force	T_{b}	Torque on bit
F_{f}	Friction force	T_{c}	Resultant torque corresponding to the internal friction force
F_{i}	Internal force	T_{e}	External torque
F_{c}	Internal friction force	T_{i}	Internal torque
F_{R}	Resultant force	U_{b}	Axial displacement of the ASST lower part
I_{b}	Inertia of BHA below ASST	U_{t}	Axial displacement of the ASST upper part
K_{b}	ASST axial spring stiffness	W_{b}	Weight on bit

1. Introduction

Nonlinear systems with discontinuities or non-smooth systems [1] have complex dynamic behaviour and they are widely used to describe phenomena observed in science and engineering. Mathematically, dynamics of these systems can be defined in terms of multidimensional flows, where a system is analysed in global hyperspace composed of smooth subspaces. As the system dynamics evolves, a trajectory passes through neighbouring subspaces and the global solution is obtained by matching the local solutions on the connecting hypersurfaces [2]. General methodology of describing and solving non-smooth dynamic systems based on the Fillipov's approach [3] can be found, for example in [1], and it can be used to analyse systems with impacts and dry friction. Well known studies include investigations of dynamics of impact oscillators [4, 5] and systems with friction [6, 7], also systems where impacts and friction occur simultaneously [8–10].

Non-smooth dynamical systems are associated with various engineering applications such as rotor-dynamics [11, 12], gear boxes [13], jarring in drill-strings [14] and Resonance Enhanced Drilling (RED) [15,

16], to name a few. In all these examples, mechanics of considered problems and(or) kinematic constraints result in change of the governing equations as the system goes from one mode of operation to another, and therefore their mathematical models belong to the class of non-smooth systems. An anti stick-slip tool (ASST) used to enhance drilling performance [17, 18] is another example of an engineering system, where both friction and motion limiting constraints are present and an interplay between them allows to achieve the desired function of the tool. A robust mathematical modelling and in depth investigation of this system is required to optimise its performance and design. So far only limited attempts have been made to describe such systems (see e.g. [19]) and a further work is needed to attain fundamental and practical insights. In this study, the background to ASSTs is given and the new mathematical model is proposed.

A drill-string is an essential component of any downhole drilling installation and it exhibits a highly complex dynamic behaviour due to strong geometrical and material nonlinearities. Axial, lateral and torsional vibration are present during its operation, and in some cases fully coupled responses including self-excited oscillations can significantly reduce drilling efficiency [20, 21]. Specifically, a severe form of torsional vibration known as stick-slip can cause fatigue or catastrophic failures. Furthermore, stick-slip oscillations can occur due to different reasons including a low torsional stiffness of a drill-string or an excessive axial force. This often results in a drill-bit being stalled instead of rotating with a constant velocity [22] and this is mainly due to the nonlinearities of bit and rock interactions [20, 21, 23, 24]. Therefore, in order to protect a drill-string and to enhance rates of penetration, stick-slip oscillations should be suppressed [24–26].

Numerous investigations have been conducted to study stick-slip vibration both numerically and experimentally. A simple torsional pendulum model is often used to represent a dynamical system exhibiting stick-slip [27, 28] whereas a coupled torsional and axial pendulums [29–32] can provide a refined description and a better insight into the system behaviour. In such models, the self-excited vibration of stick-slip nature are often caused by presence of frictional elements describing drill-bit and rock interactions. In general, there are many dry friction models [6] and a common approach is to use a simple dry friction model to describe the drill-bit and rock interactions [33]. A combination of the dry friction and exponential decay, where the frictional force decreases from the static to dynamic value is also widely used, where energy dissipation in the system is usually described by a viscous damping [27, 28]. The model proposed by Navarro Lopez and Cortes [28] was developed based on the experimental studies performed by Brett [34], Dunayevsky and Abbassian [35], and Pavone and Desplans [33]. Also, Stribeck friction model [36], a pre-sliding non-reversible damping [37, 38] have been often used. A simple

static approach to model the hysteresis of friction force with micro slidings was proposed by Powell and Wiercigroch [39] and Wiercigroch *et al.* [40].

An accurate description of the relationship between the Weight On Bit (WOB) and Torque On Bit (TOB), is vital for obtaining a meaningful prediction of the stick-slip oscillations in drill-strings. A simple model presented in [41] was developed first for the roller-cone drill-bit using both laboratory and field drilling data. Those studies were later improved to describe the bit-rock interactions more accurately [42]. The relation between WOB and TOB was defined for individual cutter with the aim of predicting and interpreting the drilling responses [43]. An insightful review on different models covering related topics such as wear mechanism, whirling and rock cutting was written by Feenstra [44, 45].

To control torsional vibration with the aim of eliminating stick-slip oscillations, different approaches have been proposed over the years by industry. Those include employing the Soft Torque Rotary Systems (STRS), which uses motor current to estimate the applied torque and modify the rotary velocity or torque [46], PI-type drive velocity controllers [47], as well as ASST developed by TOMAX [17, 18]. The latter one, ASST, is a mechanical device designed to control torsional vibration by converting an excessive external torque into a retracking axial movement of the bit allowing to avoid unwanted stick phase.

A couple of attempts have been made to model a downhole drilling with an ASST in [19, 48], where a torsional pendulum model with a motion constraint converting rotational displacement into axial displacement were used. These studies considered an ASST incorporated into a drill-string without a detailed modelling of an ASST itself, which has very nonlinear nature. Hence the current study aims to investigate the dynamics of an ASST under various loadings scenarios when the tool is activated and non-activated during the operation, where a novel dynamic model of an ASST with four distinct states of operation is proposed and analysed. The model describes rotational and axial movements of a drill-bit connected to an ASST, under an external excitation applied to the part connected to a drill-string and for the prescribed weight and torque. The drill-string dynamics is simplified by introducing the rotational and axial velocities at top part of tool while lateral movements are not considered. The bit-rock interactions are predefined as external forces acting on the bottom part of tool mounted on a drill-bit.

The rest of the paper is organised as follows. In Section 2, the ASST is introduced and details of its internal components are described. The motion constraints and their physical meaning are also explained in this section. In Section 3, a new dynamic model is developed for the tool by considering the internal and external forces acting on the top, bottom and inside the tool. Also, the states where the tool is activated or non-activated are explained. Section 4 presents example numerical results describing the ASST behaviour in different loading scenarios whilst in Section 5 some conclusions are drawn.

2. ASST and its physical model

Stick-slip is a phenomenon caused by frictional interactions between two sliding surfaces, manifesting itself in two distinct phases, a stick where there is no relative motion between those surfaces and a slip, they move with respect to each other. The main reason for the friction to be the origin of the stick-slip phenomena is the difference between the static and dynamic friction [49] and this has been extensively investigated in the past [50–53]. A simple system experiencing stick-slip is presented in [50], where a mass attached to a spring and viscous damper is placed on a rough surface and is being pulled as shown in Figure 1(a). This model despite its simplicity is strongly nonlinear. Another widely used example of a system with stick-slip is shown in Figure 1(b), where a mass attached to a linear spring and a viscous damper, is placed on a belt moving with a constant velocity.

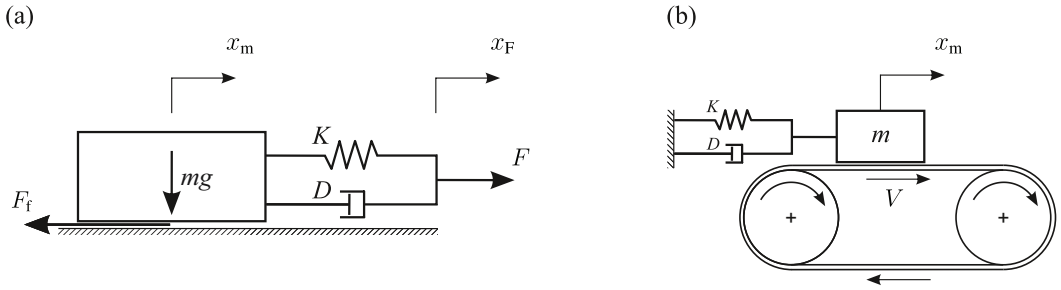

Figure 1: Examples of single degree-of-freedom systems experiencing stick-slip; (a) a lump mass connected to a linear spring and a viscous damper which can be moved when the applied force, F, is greater than the friction force, F_{f}. The Kelvin-Voight pair can make the system dynamical responses very complex and ranging from a full stop to chaotic oscillations, (b) a mass attached to a linear spring and a viscous damper that is placed on a belt moving at a constant velocity, where the friction force depends on the relative velocity between the mass and belt.

In Figure 1(a) when the mass is at rest (stick phase), an external force F is smaller than the friction force, F_{f}. And as F increases, the right hand end of the Kelvin-Voight pair moves to the right, but the mass remains motionless until the driving force exceeds the frictional resistance, $F \geq F_{\mathrm{f}}$. At this moment the mass starts moving and depending on the nature of the friction force, F_{f} can decrease from the static to dynamic friction resulting in a higher temporal velocity (slip phase) and the mass stops and if the forcing does not change, the stick-slip cycle will be repeated. In Figure 1(b) during the stick phase of the mass the velocity of the mass is equal to the velocity of belt, just if applied force to the mass by spring and damper exceeds static friction force, a transition of stick to slip will occur. And in the slip phase in accordance with the tangential velocity, friction force can be determined. In general, a change from the static to dynamic friction can be sudden or gradual and can also depend on the direction of the movement [6, 36] as shown in Figure 2. As it can be seen from Figure 2(d), considering the viscous friction results in increase of the frictional force acting on the moving mass at the higher velocities of the

mass motion [36].

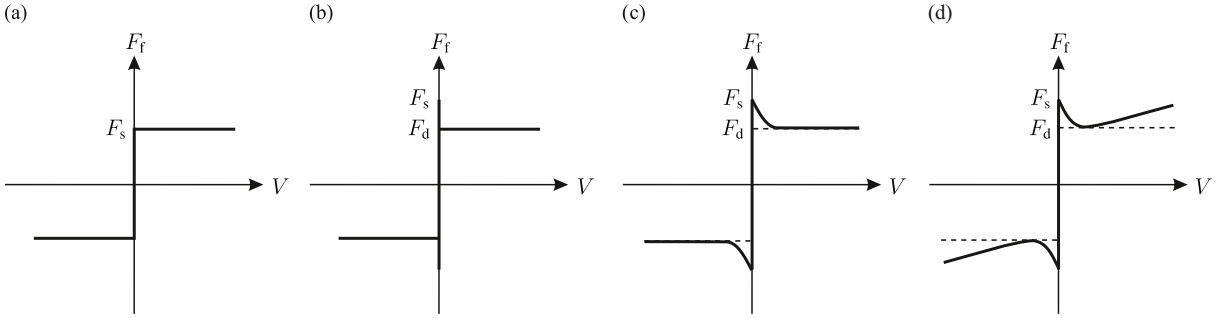

Figure 2: Common dry friction models; (a) classical Coulomb, (b) two points Coulomb, (c) exponential decay, (d) Stribeck with exponential decay and viscosity.

Torsional pendulum systems with a difference between static and dynamic friction [6, 27, 28] have been investigated in the past to study drill-string dynamics, and they provide another example of system where the friction is a source of stick-slip vibration. In this case, the bottom part of the torsional pendulum stays in the stick phase, while the top side is rotating and the torque is being stored in the spring mimicking the drill-string. The resistive torque between the drill-bit and a drilled formation, T_r, will increase as the drill-string twists until the frictional torque reaches its maximum value and then the drill-bit starts to slide, and it overshoots with a high velocity. Finally, the drill-bit stops and the cycle can be repeated over and over [27, 28].

In this study we focus on describing the dynamics of the ASST which later on can be integrated into the global model, where drill-string, drill-bit and drilled formation are considered. 3D view of a typical ASST is shown in Figure 3, where its location within drill-string is marked. A typical ASST shown in Figure 4(a) consists of two main components, namely a compressed spring and helical spline, which control the relative motions between the drill-string and drill-bit to suppress stick-slip.

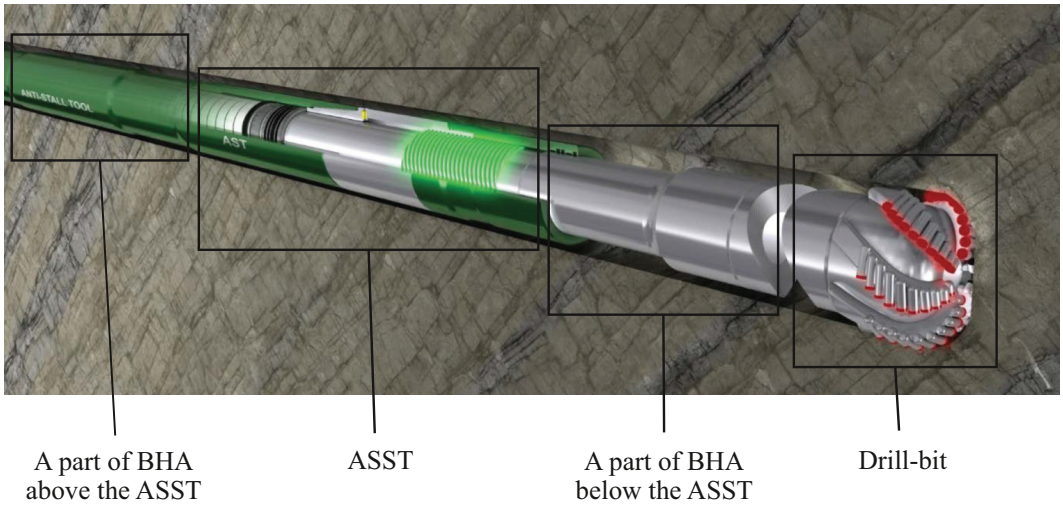

Figure 3: 3D view of an ASST placed between a BHA and a drill-bit. The BHA rotates and pushes the drill-bit in the process of a wellbore creation and if the TOB acting on the drill-bit is too large which occurs during stick phase, the ASST is activated and retracts thanks to a spline reducing the WOB and effectively the TOB. ASST enables the drill-bit and BHA to have a relative motion.

As mentioned earlier an ASST is designed to convert the excessive external torque into the axial movement of the drill-bit providing a reduction in the weight on bit, WOB, by shortening the drill-string length.

As can be seen from Figure 3, the ASST is mounted in a Bottom Hole Assembly (BHA). For normal drilling conditions, the ASST is not activated and the drill-bit is steadily progressing forward. Once the resistance torque at the rock and drill-bit interface exceeds the internal torque of ASST, the tool is activated and retracts thanks to the helical spline, which consequently shortens the drill-string reducing the WOB and in turn also the TOB. The axial retraction of the drill-bit, L, for one revolution of the tool, 2π, depends on the geometry of the spline. The ratio $\alpha = L/2\pi$ determines the relation between the relative rotational ($\Delta\Phi = \Phi_\mathrm{t} - \Phi_\mathrm{b}$) and axial ($\Delta U = U_\mathrm{t} - U_\mathrm{b}$) displacements. Note that subscripts (t) and (b) denote the motions at the top and bottom, respectively. If the angle of the spline thread is θ and the mean radius of spline thread is r_s, the axial retraction per full revolution can be defined as $L = 2\pi r_\mathrm{s} \tan\theta$ and therefore the ratio is $\alpha = r_\mathrm{s} \tan\theta$. It is assumed that the relative axial displacement of the ASST length, ΔU, is zero when the tool is fully expanded and the relative rotational displacement, $\Delta\Phi$ is initially zero. Then, the relation between the relative axial and rotational displacements is

$$\Delta U = \alpha \Delta\Phi. \tag{1}$$

A 3D view and physical model of the considered system are presented in Figure 4, for which at the top of the ASST, rotational and axial velocities are prescribed. The lower part of the ASST together with the drill-bit having mass M_{b} and inertia I_{b}, are attached to the top part via a spline mechanism having a preloaded spring. U_{t} and Φ_{t} are the axial and rotational displacements of the upper disk and U_{b} and Φ_{b} denote corresponding ones of the lower disk. D_{b} is the damping coefficient and K_{b} represents the stiffness of the spring inside the ASST.

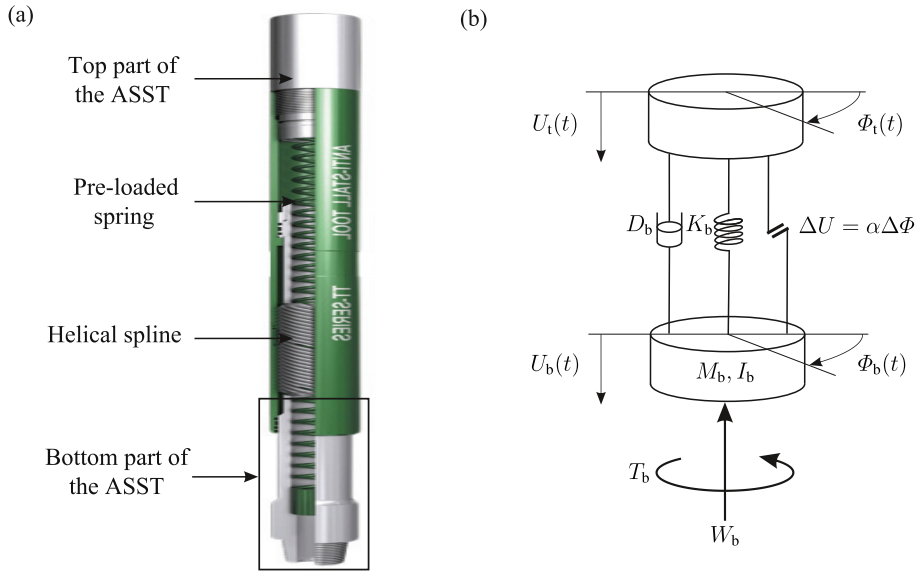

Figure 4: (a) 3D view of the ASST showing its components inside including the helical spline and axial spring (adopted from [17]), (b) physical model having the upper part and lower parts connected to each other.

3. Mathematical modelling

A mathematical model of the system containing important characteristics of the ASST has been developed in this section, where a special attention is given to the internal friction of the ASST. By dividing the tool into the top and bottom parts and considering the helical spline inside the ASST, the mechanism of ASST mimics a screw like connection. The ASST contains also an axial pre-loaded spring, which expands the tool when the external forces are lower than the internal ones. In this paper, the nonlinear bit-rock interactions will be modelled by harmonic functions acting on the bottom part of the ASST to easily test the proposed model. In the following subsections an analysis of ASST motion is presented, and the distinct states of the system motion are fully defined.

3.1. Mechanics of ASST

Major parts of the ASST consist of the helical spline connected to the drill-bit, which is coupled to the top section by means of a threaded hub. This coupling enables the system to transmit torque and motion between two parts. In the activated state, rotation of the helical spline inside the hub suppresses the excessive external torque and the axial force. A pre-loaded spring inside the ASST plays a vital role in the function of the tool. The internal spring prevents the ASST from being activated by a lower force than a threshold acting on the bit. An explanation of how the ASST works, is illustrated in Figure 5.

In this study, top of the tool is subjected to prescribed axial and rotational motion, therefore the rotational $\Phi_{\mathrm{t}}(t)$, and axial $U_{\mathrm{t}}(t)$ positions of the upper part are defined. The WOB and TOB are dependent on drilling parameters, bit geometry and drilled formation characteristics. For different drilling regimes, the values of WOB and TOB can vary significantly. Three schematics shown in Figure 5 depict a typical ASST geometry, prescribed kinematics, external and internal forces acting on and within the tool. Figure 5(a) presents both the upper and lower parts together with the preloaded spring. For the purpose of clarity all external forces acting on the upper and lower parts together are depicted in Figure 5(b) and 5(c) respectively.

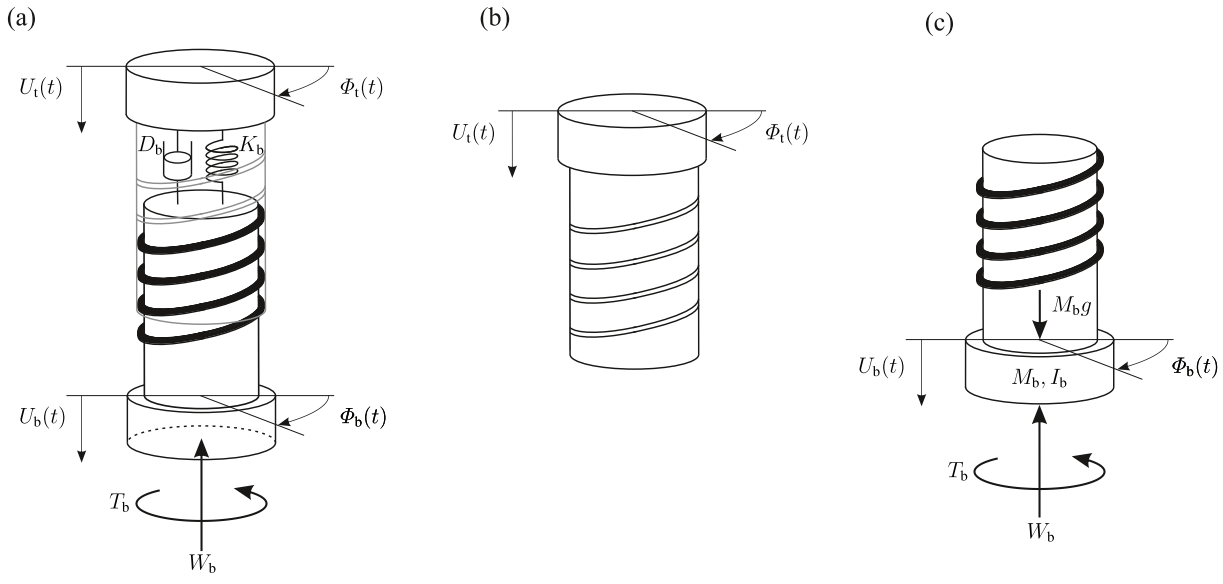

Figure 5: Schematics of the structure and kinematics of the ASST physical model showing also external forces; (a) the assembled ASST, (b) the top part containing female helical spline, (c) the bottom part with male helical spline.

The pre-load force, P, generated from the internal spring is a simple product of the spring stiffness K_{b} and the spring pre-load compression, δ_{p} as

$$P = K_{\mathrm{b}}\delta_{\mathrm{p}}. \tag{2}$$

By considering the non-activated state as the static equilibrium position of the ASST, during the activation, the resulting deflection of the axial spring is equal to axial relative displacement. Therefore, the resultant force from the spring and the viscous damper between two parts of ASST is considered as the internal force of ASST, denoted by F_{A}, which can be calculated as

$$F_{\mathrm{A}} = P + K_{\mathrm{b}}(U_{\mathrm{t}} - U_{\mathrm{b}}) + D_{\mathrm{b}}(\dot{U}_{\mathrm{t}} - \dot{U}_{\mathrm{b}}). \tag{3}$$

The internal friction force between two parts of the ASST at the helical spline is one of the most important mechanisms, however this has not been yet tackled and reported in the open literature. By considering the frictional contact in sliding surfaces of the helical spline, it would affect the dynamics of the ASST. Therefore, there are internal friction forces acting on the spline, which are caused by the movement of the upper and lower parts of ASST through the helical spline section as depicted in Figure 6.

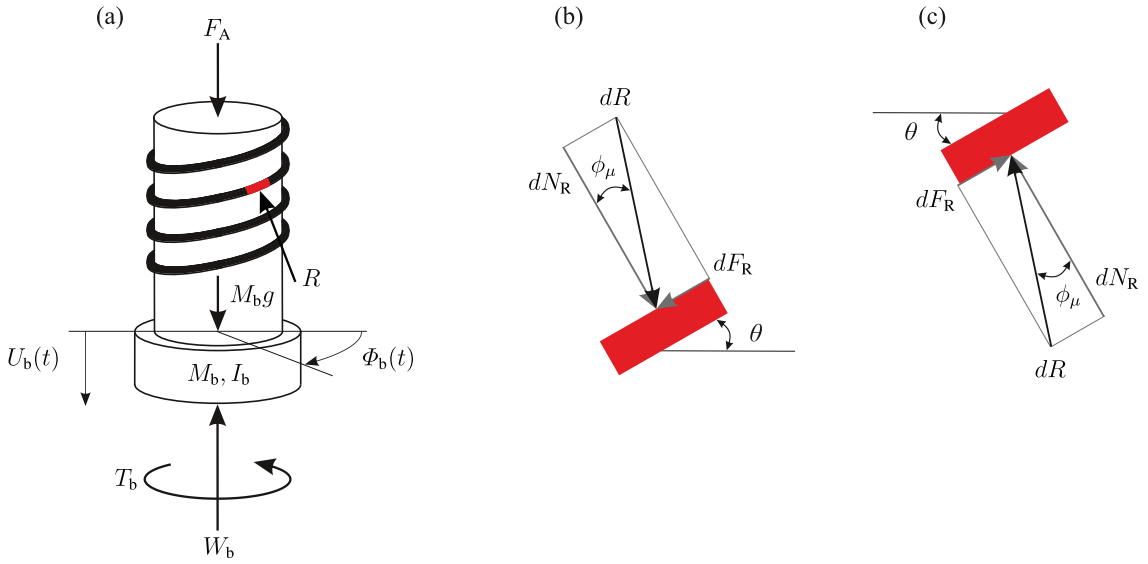

Figure 6: Internal frictional forces in the helical spline section; (a) physical model of the bottom part, (b) decomposition of the forces when the tool is being compressed where the upper surface of the male thread is engaged and normal force dN_{R} is acting downwards, (c) decomposition of forces when the tool is expanding and lower surface of the male thread is engaged and dN_{R} is upward.

In Figure 6, dR is the infinitesimal force applied on the thread due to the friction in the sliding surfaces, and dN_{R} and dF_{R} stem from the decomposition of dR. Therefore, the integral of the infinitesimal forces over the length of thread l_{t} can be expressed as $R = \int_{l=0}^{l=l_{\mathrm{t}}} dR$. The normal and friction forces are denoted as N_{R} and F_{R}, respectively. An accurate modelling of the contact mechanics on the internal helical spline should involve the Hertz contact theory, however, for the sake of simplicity and clarity, we used the simple Coulomb friction. The coefficient of friction μ and angle of internal friction can be defined as follows:

$$\phi_\mu = \tan^{-1}\mu = \tan^{-1}\frac{F_\mathrm{R}}{N_\mathrm{R}}. \tag{4}$$

It should be noted here and as shown in Figure 6, the following assumption is made, when the tool is being compressed, the upper surface of the male thread is in contact with the female thread. Therefore, the normal force acting on the male thread is directed downwards, which is shown in Figure 6(b). On the other hand, when the tool is expanding, it is assumed that the lower surface of the male thread is in contact with the female thread, hence the normal force acting on the male thread is upward. During the expansion F_R acts in the opposite direction as depicted in Figure 6(c).

According to the above assumption and considering $\theta > \phi_\mu$, the effective friction angle in both conditions shown in Figure 6, is equal to $\theta - \phi_\mu$. The direction of motion along with the type of contact changes, so the sign of friction coefficient would be same all the time. Therefore, the internal friction force F_c in vertical direction and the resultant torque T_c can be calculated as

$$F_\mathrm{c} = \pm R\cos(\theta - \phi_\mu), \;\; T_\mathrm{c} = \mp r_\mathrm{s} R\sin(\theta - \phi_\mu). \tag{5}$$

In Eq. (5) plus/minus sign ($\pm$) denotes the directions of internal friction force for compression/expansion states of the tool. When we use two signs such as ($\pm$, $\mp$) the upper sign indicates compression state and the lower sign refers to the expansion state. Therefore, for the compression state, F_c has the same sense of direction as the axial movement ($+$), and the sense of rotation of T_c is opposite to the sense of rotation ($-$), and vice versa for the expansion state. After accounting for the internal and external forces, the equations of motion can be formulated from the second Newton's law

$$M_\mathrm{b}\ddot{U}_\mathrm{b} = P + K_\mathrm{b}(U_\mathrm{t} - U_\mathrm{b}) + D_\mathrm{b}(\dot{U}_\mathrm{t} - \dot{U}_\mathrm{b}) \pm R\cos(\theta - \phi_\mu) + M_\mathrm{b}g - W_\mathrm{b}, \tag{6}$$

$$I_\mathrm{b}\ddot{\Phi}_\mathrm{b} = \mp R r_\mathrm{s}\sin(\theta - \phi_\mu) - T_\mathrm{b}. \tag{7}$$

By deriving the equivalent expression for R from the Eq. (6), and substituting it into the Eq. (7), we can rewrite Eq. (7) in following form

$$I_\mathrm{b}\ddot{\Phi}_\mathrm{b} = -r_\mathrm{s}\tan(\theta - \phi_\mu)\left(M_\mathrm{b}\ddot{U}_\mathrm{b} - P - K_\mathrm{b}(U_\mathrm{t} - U_\mathrm{b}) - D_\mathrm{b}(\dot{U}_\mathrm{t} - \dot{U}_\mathrm{b}) - M_\mathrm{b}g + W_\mathrm{b}\right) - T_\mathrm{b}. \tag{8}$$

It should be noted that, to simplify the presentation in the rest of the paper we use r_i to explain

notation $r_{\mathrm{s}}\tan(\theta-\phi_{\mu})$. Moreover, by having the motion constraint $(U_{\mathrm{t}}-U_{\mathrm{b}})=\alpha(\Phi_{\mathrm{t}}-\Phi_{\mathrm{b}})$, the equations of motion can be rewritten in terms of Φ_{b}, Φ_{t} and U_{t}. Finally, Eq. (9) presents the governing equation for coupled axial and torsional dynamics of the activated ASST considering the internal friction

$$(M_{\mathrm{b}}\alpha r_{\mathrm{i}}+I_{\mathrm{b}})\Delta\ddot{\Phi}+D_{\mathrm{b}}\alpha r_{\mathrm{i}}\Delta\dot{\Phi}+K_{\mathrm{b}}\alpha r_{\mathrm{i}}\Delta\Phi=M_{\mathrm{b}}r_{\mathrm{i}}\ddot{U}_{\mathrm{t}}+I_{\mathrm{b}}\ddot{\Phi}_{\mathrm{t}}+r_{\mathrm{i}}W_{\mathrm{b}}+T_{\mathrm{b}}-r_{\mathrm{i}}(P+M_{\mathrm{b}}g). \tag{9}$$

In the modelling of ASST, the emphasis is mostly put on the torsional vibration and the torque evolution, however, in order to capture the axial motion and force evolution of system, one can also rewrite Eq. (9) in terms of U_{b}, U_{t} and Φ_{t}, so alternative form of this equation is

$$(M_{\mathrm{b}}+\frac{I_{\mathrm{b}}}{r_{\mathrm{i}}\alpha})\Delta\ddot{U}+D_{\mathrm{b}}\Delta\dot{U}+K_{\mathrm{b}}\Delta U=M_{\mathrm{b}}\ddot{U}_{\mathrm{t}}+\frac{I_{\mathrm{b}}\ddot{\Phi}_{\mathrm{t}}}{r_{\mathrm{i}}}+W_{\mathrm{b}}+\frac{T_{\mathrm{b}}}{r_{\mathrm{i}}}-(P+M_{\mathrm{b}}g). \tag{10}$$

After deriving the equations of motion, the torques acting on the system can be categorised into three groups of external, internal and activation torques and computed from Eqs (11-13):

$$T_{\mathrm{e}}=r_{\mathrm{i}}M_{\mathrm{b}}\ddot{U}_{\mathrm{t}}+I_{\mathrm{b}}\ddot{\Phi}_{\mathrm{t}}+r_{\mathrm{i}}W_{\mathrm{b}}+T_{\mathrm{b}}, \tag{11}$$

$$T_{\mathrm{i}}=T_{\mathrm{a}}+D_{\mathrm{b}}\alpha r_{\mathrm{i}}\Delta\dot{\Phi}+K_{\mathrm{b}}\alpha r_{\mathrm{i}}\Delta\Phi, \tag{12}$$

$$T_{\mathrm{a}}=r_{\mathrm{i}}(P+M_{\mathrm{b}}g), \tag{13}$$

where T_{e} is the sum of the external torques, which are compressing the ASST, T_{i} is the total internal torque, which helps the tool to expand based on stored energy and T_{a} is the minimum torque required to activate the ASST. The relative rotational acceleration can be obtained in following form

$$\Delta\ddot{\Phi}=\frac{T_{\mathrm{e}}-T_{\mathrm{i}}}{M_{\mathrm{b}}\alpha r_{\mathrm{i}}+I_{\mathrm{b}}}. \tag{14}$$

Looking at Eq. (14), it is worth to point out here that relative rotational acceleration affects the relative velocities of the top and bottom parts that can lead to change between the ASST states.

3.2. ASST distinct states

The operational responses of the ASST can be classified into two general states, activated and non-activated. When the ASST is not activated, the top and bottom parts of the tool together with the BHA and the drill-bit rotate with the same velocity and can be regarded as a rigid body. In other words, non-activated state is characterized by zero relative velocity. Note that Eq. (9) is only valid for the

activated state as for the non-activated one, both the upper and lower parts of the tool move together as a rigid body and its motion is governed by the prescribed kinematics of the upper part. According to the governing equation of motion, the condition to attain the activated state is to overcome the internal forces and torques of the ASST. Therefore, the tool remains in the non-activated state unless the external forces exceed the threshold value.

Non-activated state. The tool is deactivated if there is no relative motion of two parts. In the non-activated state, the external torque must be smaller than the activation torque ($T_{\mathrm{e}} \leq T_{\mathrm{a}} = T_{\mathrm{i}}$). In this state, the axial and rotational motion of the bit are same as the top part. Therefore, the relative rotational and axial motion velocities are zero ($\Delta\dot{\Phi} = 0$, $\Delta\dot{U} = 0$) and the tool is fully expanded and two parts act as a rigid body. The mathematical description of non-activated state can be defined as

$$\Phi_{\mathrm{b}}(t) = \Phi_{\mathrm{t}}(t), \;\; U_{\mathrm{b}}(t) = U_{\mathrm{t}}(t). \tag{15}$$

Activated state. This state occurs where the motions of the upper and lower part of the ASST differ, which means either displacements, velocities or both are different. Mathematically, it can be described as two inequalities ($\Delta\Phi > 0$, $\Delta U > 0$). When the external torque exceeds the activation torque, ASST state, would change from non-activated to activated state. During the activated state the relative displacement and velocity are not zero and need to be calculated from the Eq. (14). Accordingly, governing equation of activated state can be reformulated as below

$$\ddot{\Phi}_{\mathrm{b}}(t) = \ddot{\Phi}_{\mathrm{t}}(t) - \frac{T_{\mathrm{e}} - T_{\mathrm{i}}}{M_{\mathrm{b}}\alpha r_{\mathrm{i}} + I_{\mathrm{b}}}. \tag{16}$$

When the velocity of the bit is smaller than the velocity of top ($\Delta\dot{\Phi} > 0$), tool is compressing and when the velocity of bit is greater than the velocity of top ($\Delta\dot{\Phi} < 0$), the tool is expanding. The third state of activation state can be named as the transient equilibrium in which ($\Delta\dot{\Phi} = 0$). For the activated state, the balance between the internal and external torques and the relative velocity, determines the motion of the tool. In this condition, where the tool is activated, there are 3 distinct sub-states which are described below:

- **Compression ($\Delta\dot{\Phi} > 0$).** During the compression state, the bit retracts from the borehole and rotates with a lower rotational velocity than the upper part which is determined by the force equilibrium and can be controlled by the inclination angle of the spline. The relative rotary motion between the lower and upper parts is opposite to the rotation of the BHA.

- **Transient equilibrium ($\Delta\dot{\Phi} = 0$, $\Delta\Phi > 0$).** In this state, the tool acts in similar way for the non-activated state but with a new equilibrium described by non zero relative displacement between the upper and the lower parts of the ASST.

- **Expansion state ($\Delta\dot{\Phi} < 0$).** Due to reduction of the external torque, the system tends to return to its initial position where the tool is fully expanded. When the stored component of the internal torque exceeds the external torque, the expansion state of the ASST starts. In this state the bottom part velocity is greater than velocity of the upper one, $\Delta\dot{\Phi} < 0$. The tool expands until it reaches the fully expanded position for which $\Delta\Phi = 0$ and the tool goes back to the non-activated state.

Table 1 summarises all states described above listing the necessary kinematic conditions, which are used to develop the mathematical model. It should be noted that, due to the existence of the inertial torque during the activated state, the torque conditions cannot be fully described but for the non-activated state the condition $T_\mathrm{e} < T_\mathrm{a}$ is necessary. A comparison of the internal and external torques indicates the direction of acceleration, however, it cannot be used for description of the distinct states during the activation of the ASST.

Table 1: Four states of the ASST operation and corresponding kinematic conditions

State	Kinematic conditions
Non-activated	$\Delta\dot{\Phi} = 0$, $\Delta\Phi = 0$
Activated in compression	$\Delta\dot{\Phi} > 0$
Activated in transient equilibrium	$\Delta\dot{\Phi} = 0$, $\Delta\Phi > 0$
Activated in expansion	$\Delta\dot{\Phi} < 0$

Moreover, there are some particular conditions, in which the system exhibits complex behaviours. As explained earlier, there are certain justifications as well as reasons which lead the system to enter into a specific state. Although the reason for activation of the tool is ($T_\mathrm{e} > T_\mathrm{a}$) where the compression starts, the tool can stay in compression state even if ($T_\mathrm{e} < T_\mathrm{a}$). This happens due to the inertial torques and as long as inertial torque exists tool remains in compression state and it takes a short period of time to go to the transient equilibrium state, where the relative velocity becomes zero ($\Delta\dot{\Phi} = 0$). In fact, this delay happens in order to overcome the inertia and change the direction of movement. A similar delay can be seen when the tool is expanding where ($T_\mathrm{e} < T_\mathrm{a}$) but ASST does not enter into the non-activated state. Because the tool is not fully expanded yet or ($\Delta\Phi > 0$), so expansion continues to reach into initial position where ($\Delta\Phi = 0$). A detailed explanation of this behaviour will be given in the next section.

4. Numerical simulation and model evaluation

In this section, the dynamic responses of the ASST are obtained numerically using a combination of the brute force numerical simulation and the kinematic conditions. A custom made numerical algorithm has been developed and a code generated in MATLAB. For all the three activated states, the direct numerical integration of Eq.(16) by employing the forth order Rung-Kutta algorithm takes place. For the non-activated state, the ASST motion is governed by the kinematic relations. In order to have a full control of the computational accuracy and to follow the system passing through all four states, we have employed a custom made fixed step Runge-Kutta algorithm. A general scenario has been designed to evaluate the system responses through different states explained in Subsection 3.1. Additionally, it is important to use reasonable parameters which reflect the ASST response in conditions close to the reality. The parameters are used to model the ASST are taken from [19], which are close to the working range values. The parameters values used for the numerical simulations are given in the Table 2. Since the behaviour of the ASST is controlled by the internal spring, therefore the spring stiffness and the pre-load should be included in the parametric studies given in this section.

Table 2: Parameters used for numerical simulation of ASST

Parameter	Symbol	Magnitude	Unit
Mass of BHA below ASST	M_{b}	1.11×10^4	kg
Inertia of BHA below ASST	I_{b}	60.8	$kg.m^2$
ASST axial spring stiffness	K_{b}	9.5×10^5	$\frac{N}{m}$
ASST axial damping	D_{b}	0	$\frac{N.s}{m}$
Constraint constant	α	0.081	m
Lead angle	θ	$\frac{\pi}{4}$	rad
Static pre-load	P	1×10^5	N
Mean radius of thread	r_{s}	0.081	m
Friction coefficient of thread	μ	0.19	$-$

4.1. Typical periodic responses

In order to validate the developed mathematical model of the ASST and to see a manifestation of all four distinct states, we have assumed the following boundary, kinematic and loading conditions. The tool will rotate with constant velocity with no axial movement at upper part. On the bottom part we apply W_{b} and T_{b}, which have static and dynamics components. Rotation of top is $\Phi_{\mathrm{t}}(t) = \pi t$ and the

axial displacement of the top disk is zero. The choice of values W_{b} and T_{b} is dictated by a need to see all distinct states, therefore, harmonic nature of variation is employed for simplicity. The prescribed W_{b} and T_{b} are harmonic functions with constants chosen as $W_b = 10^4(8 + \sin(2\pi t))$ and $T_b = 10^3(8 + \sin(2\pi t))$. The following results are obtained by employing the parameters given in Table 2 for the general case. In order to reduce the complexity of response and explain different states of ASST operation easily, we set the coefficient of the damping to zero. Figure 7 shows time histories of axial and rotational motion of the upper and lower parts also evolutions of external, internal and activation torques as well as axial forces in the ASST.

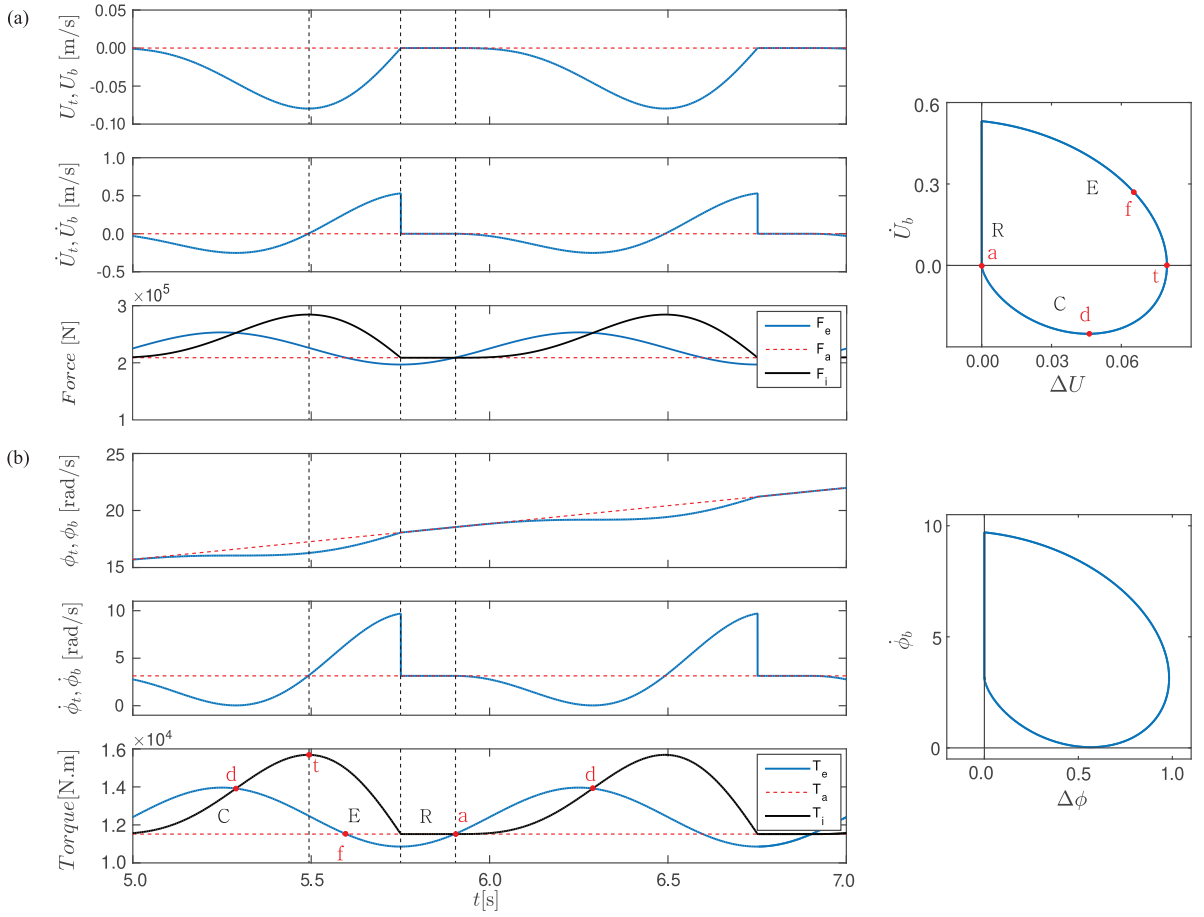

Figure 7: ASST response when top rotates with a constant velocity and axial velocity is zero. (a) Time histories for axial motion where the red dotted lines represents the top and blue lines are bottom motions, evolutions of axial forces and phase portrait, (b) time histories for rotational motion, evolutions of torques and phase portrait.

Figure 7 presents typical periodic response of the system. In Figure 7(a) dash vertical lines indicate boundaries between different states of the system response which are marked by letters C, E and R in one period of the system response. Small letters d, t, f and a are placed in the key points of the response.

In Section (C), ASST is activated and it is in compression state because the relative velocity is greater than zero ($\Delta\dot{\Phi} > 0$, $\Delta\dot{U} > 0$). As it can be observed from Point (a) to Point (d), the external torque is greater than the both activation and internal torques ($T_{\mathrm{e}} > T_{\mathrm{i}} > T_{\mathrm{a}}$), which justifies the compression state. Therefore, the upward movement of the bottom part leads the spring to be compressed and to create a force in the opposite direction so that the T_{i} increases. From the Point (d), value of T_{i} is greater than T_{e}, therefore the relative axial velocity decreases and the bottom part of the tool slightly decelerates until the compression state ends. This point is marked by Point (t) on phase portrait, which corresponds to the dashed line between Section (C) and (E). In addition, Point (t) is the transition from compression to expansion and as it can be seen from Figure 7 velocity values of two parts are equal, which means ($\Delta\dot{\Phi} = 0$, $\Delta\dot{U} = 0$). In Section (E) tool is still activated ($\Delta\Phi > 0$, $\Delta U > 0$) and it is in expansion state ($\Delta\dot{\Phi} < 0$, $\Delta\dot{U} < 0$). At Point (f), T_{e} is less than T_{a} but since the tool is not fully expanded, expansion continues until the tool reaches the initial axial position ($\Delta U = 0$). The delay between Point (f) and start of non-activated state (R) depends on the variation trends of external and inertial forces of the ASST. Fully expanded position is in fact equivalent to the non-activated state. In other words, the sudden change (jump) in response of the system signifies that tool enters non-activated state ($\Delta\Phi = \Delta U = 0$) and ASST has a rigid body motion. Section (R) is where the ASST is non-activated and because T_{e} is less than T_{a} and the tool is fully expanded. Until Point (a), which is located in the (zero-zero) point at the phase portrait, the tool stays non-activated and acts like a rigid body. In this section, the motion of the bottom is same as the top. Point (a) is considered as the activation point, and after this point T_{e} gets greater than T_{a} which makes the tool to get activated and enter the compression state again (Section (C)).

In order to test the model further, we introduce three cases that in each one only one parameter changes while the others are kept constant. The example presented in Figure 7 has been considered as a benchmark case to be compared with other cases in order to analyse the dynamical responses by changing the key parameters. For this purpose, in the first case influence of pre-load is analysed, which ranges form 0.5×10^5 to $1.25 \times 10^5 N$, and in the second case stiffness of the internal spring changed form 9.5×10^5 in benchmark case to $9.5 \times 10^6 \frac{N}{m}$.

4.2. Effect of pre-load

Figure 8(a) shows the results when the pre-load is 0.5×10^5 N, and Panels (b) and (c) present the dynamical responses for the cases in which the pre-load force is increased to 1×10^5 and 1.25×10^5 N, respectively. The Eq. (13) indicates that any changes in the spring pre-load force directly affects the

activation torque. Therefore, by decreasing the pre-load force, the activation torque will decrease and vice versa.

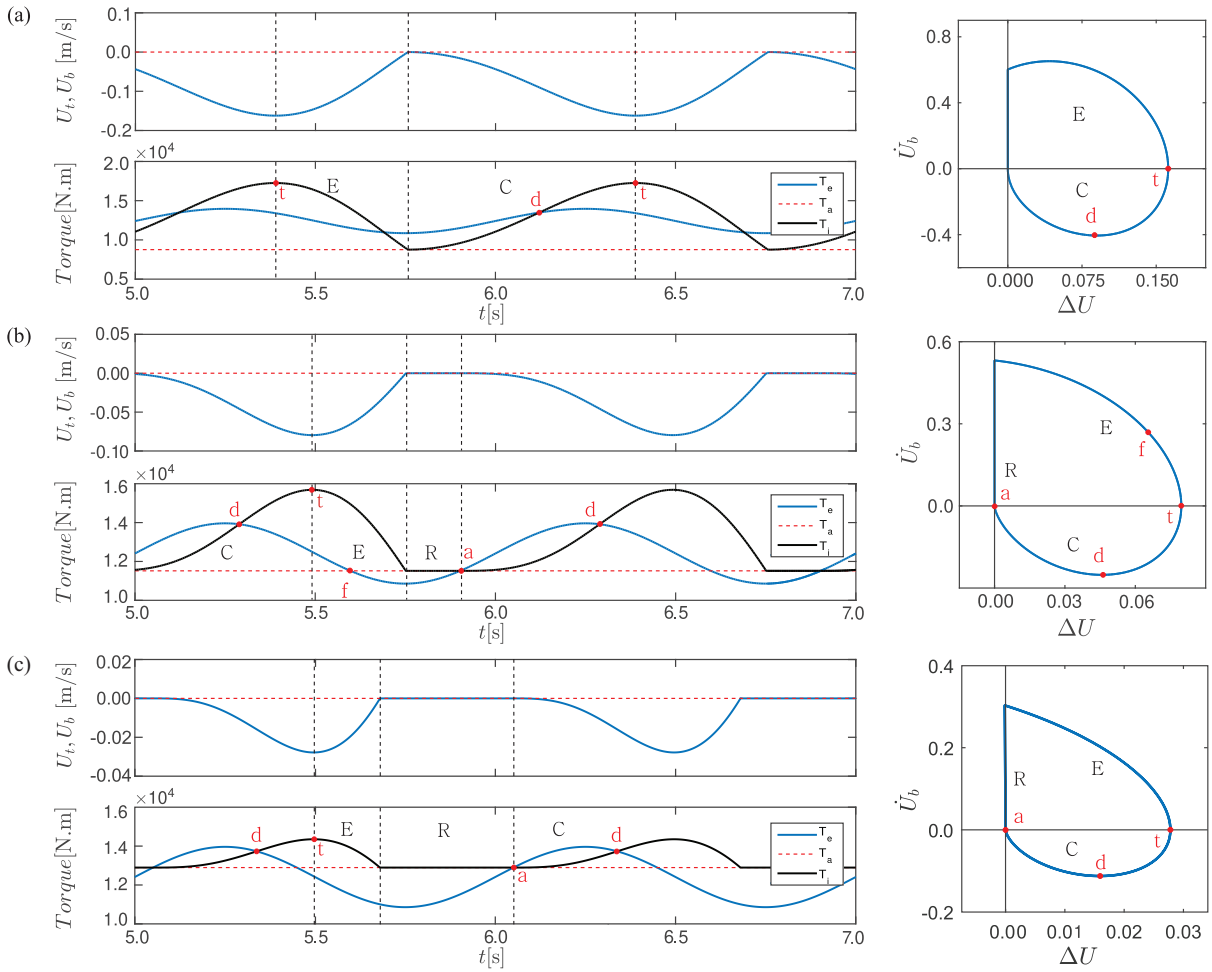

Figure 8: Time histories for axial motion, evolutions of torques and phase portraits for axial motion when the pre-load is varying; (a) $P = 0.5 \times 10^5$ N, (b) $P = 1 \times 10^5$ N, (c) $P = 1.25 \times 10^5$ N.

In the Figure 8(a), it can be seen that system stays in the activation state all the time. As a matter of fact, the rigid body motion will not occur since the value of T_{e} remains greater than T_{a} all the time. In Section (C), the tool is compressing but after Point (d) when the deceleration starts, T_{i} exceeds the T_{e}, therefore the balance of the forces changes and this makes the upward axial velocity of the bit to decline and eventually the compression stops. Point (t) is the transient equilibrium which is marked in phase portrait and time histories.

In Figure 8(c), starting form Point (a), system enters the compression state. The compression continues till Point (t) which is the transient equilibrium and the tool starts to be expanded right after that. As can be seen in Section (E), since the inertial components still exist, the tool is activated even though

T_e is smaller than T_a. Section (R) is where ASST is non-activated. Therefore, all the four distinct states can be observed for this case. Results show that lower values of pre-load force makes ASST to stay in the activation state on the lower external torque values. Conversely, presence of large downward pre-load force on the bottom part of ASST resists the higher external torques. Although higher values of pre-load prevent the ASST from large amplitude oscillations, high pre-loads can lead to non-activated states and limit effectiveness of the tool.

4.3. Effect of stiffness

When the ASST is compressed, due to the upward movement of the lower part, the internal spring is compressed and generates a force in the opposite direction. According to Eq. (12), internal torque is a function of spring force and hence, by increasing the spring stiffness, deflection of spring will significantly influence the internal torque. Consequently, during the activated state, T_i gets more sensitive to axial movement of the bit. Therefore, any small axial movement can result in change of the internal torque T_i to a higher value. This makes the internal torque T_i to exceed the external torque T_e rapidly and changes the value and direction of axial acceleration of the bottom part. Therefore, the tool can expand and compress more frequent in smaller intervals. Figure 9 shows the system response when the internal spring stiffness of the ASST is increased from 9.5×10^5 of benchmark case to 9.5×10^6 $\frac{N}{m}$.

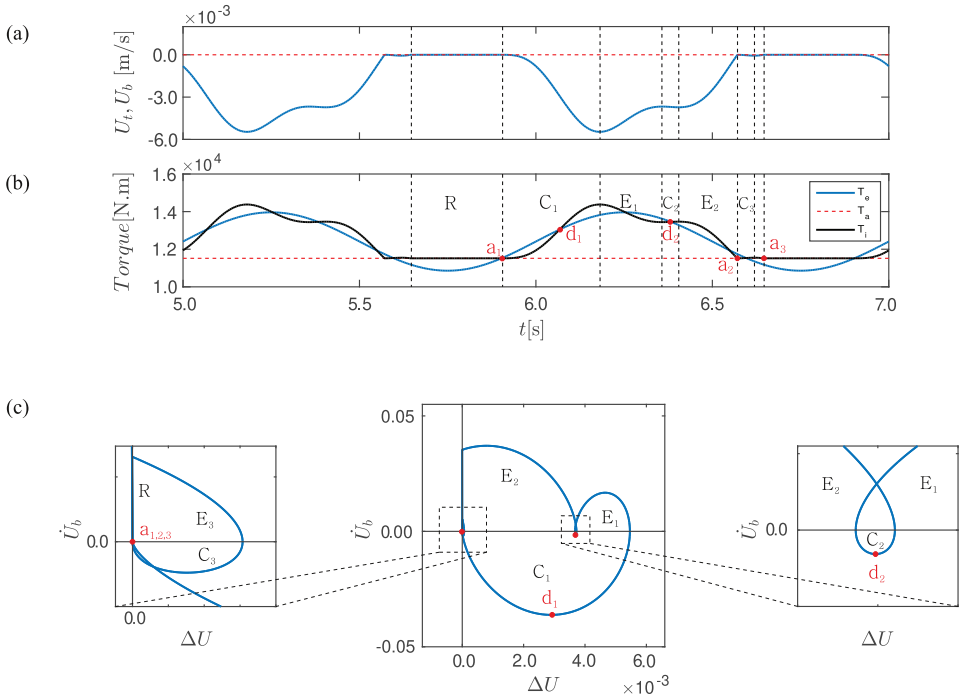

Figure 9: ASST response when the internal spring stiffness is increased from 9.5×10^5 to 9.5×10^6 $\frac{N}{m}$; (a) time histories for axial motion, (b) evolutions of torques, (c) phase portrait for axial motion, the zoomed sections are also small compression and expansion zones which have been plotted.

Figure 9 demonstrates that during one period, the value of T_{i} oscillates around T_{e}. Initially, it is going from Point (a_1) when the activation starts, the value of T_{e} is greater than T_{a} so that the ASST is being activated and compressed. Thereafter, as a result of the spring compression, T_{i} exceeds the T_{e}, however, due to the inertia of the bit, the compression continues until the inertia of the bottom part vanishes. In Section (E_1) system is expanding, however T_{i} is not necessarily greater than T_{e} through out this section. As it can be seen, almost in the middle of this interval T_{e} exceeds T_{i}. This change in the balance between torques causes a deceleration of the bottom part of tool. Section (C_2) shown as a zoomed-in view of phase portrait at right side of Panel (c), indicates the condition in which system enters the compression state and immediately returns to expansion state during a short period of time. In Section (C_2), intersections with horizontal axis indicates the transient equilibrium states. In Section (E_2) system expands until is fully elongated $(\Delta U = 0)$. Then the tool acts like a rigid body and the velocities of the top and bottom will be same $(\Delta \dot{U} = 0)$. In zoomed-in view of phase portrait at left side, the small counter-clockwise circle, marked by C_3 and E_3, exhibits another compression/expansion cycle. At the final activated state, the internal torque changes with a higher rate than external torque and therefore after Point (a_2) the bit experiences a small deflection only. Therefore, it can be concluded that, the advantage of increasing

spring stiffness limits the amplitude of oscillations, however, it makes the tool more sensitive to external load variations.

5. Closing remarks

In this work, we have developed and tested a new mathematical model of the Anti Stick-Slip Tool (ASST), which is used in drill-string arrangements to suppress or even completely eliminate dangerous stick-slip vibration often occurring during rotary drilling. The ASST is a mechanical device comprised of two main parts forming a screw-nut pair, and connected to each other via a helical spline with a pre-loaded spring between them. Practically, the ASST translates a rotary relative motion of the screw-nut pair to an axial one when an external torque is larger than the internal one within the ASST, resulting in an axial relative displacement, which in effect shortens a drill-string and prevents a drill-bit from getting stuck.

The developed mathematical model identifies and describes four distinct states of operation, namely, Non-Activated, Activated-Compression, Activated-Transient Equilibrium and Activated-Expansion. These four states originate from two main states when the ASST is activated and non-activated, which are due to the ASST design having the pre-loaded spring and the helical spline, which mathematically represents a constraint. As the result, two states are described by different equations, specifically, representing a single degree-of-freedom system when the tool is activated and a prescribed kinematic motion when the tool is not activated. The model also defines the switch between those two main states and therefore it accounts for non-smooth dynamic nature of the stick-slip phenomena and the mechanics of the ASST.

The ASST mathematical model has been systematically tested by calculating evolutions of motion and forces describing the tool for various system parameters and initial conditions which trigger four distinct states. Specifically, we have computed time evolutions of the axial and rotational displacements and velocities, and the axial force and torque. All four distinct states were observed and the characteristic points on these evolutions were identified and named. We also conducted a short parametric study looking at the effects of the internal spring pre-load and its stiffness showing complex activation patterns.

The undertaken modelling and obtained results are first steps to fully understand the mechanics of the ASST, where an interplay between the dry friction and the pre-load needs to be unveiled. This study should help to understand all intricacies of the ASST operation and it can be used to create a more realistic model by relaxing simplifying assumptions to describe the operation of the tool with more fidelity. The next steps in the future studies will be relaxing simplifying assumptions, adding bit-rock interactions and incorporating the ASST model with a drill-string.

References

[1] M. Wiercigroch and B. Kraker. *Applied Nonlinear Dynamics and Chaos of Mechanical Systems with Discontinuities, Nonlinear Science Series A*, volume 28. World Scientific, Singapore, 2000.

[2] E. Pavlovskaia and M. Wiercigroch. Low-dimensional maps for piecewise smooth oscillators. *Journal of Sound and Vibration*, 305(4):750–771, 2007.

[3] A.F. Filippov. Differential equations with discontinuous right-hand side. *American Mathematical Society Translations*, 42(2):199–231, 1978.

[4] F. Peterka and J. Vacík. Transition to chaotic motion in mechanical systems with impacts. *Journal of Sound and Vibration*, 154(1):95–115, 1992.

[5] D. J. Wagg and S. R. Bishop. Application of non-smooth modelling techniques to the dynamics of a flexible impacting beam. *Journal of Sound and Vibration*, 256(5):803–820, 2002.

[6] J. Wojewoda, A. Stefański, M. Wiercigroch, and T. Kapitaniak. Hysteretic effects of dry friction: modelling and experimental studies. *Philosophical Transactions of the Royal Society A: Mathematical, Physical and Engineering Sciences*, 366(1866):747–765, 2008.

[7] A. Saha, M. Wiercigroch, K. Jankowski, P. Wahi, and A. Stefański. Investigation of two different friction models from the perspective of friction-induced vibrations. *Tribology International*, 90:185–197, 2015.

[8] C. J. Begley and L. N. Virgin. Impact response and the influence of friction. *Journal of Sound and Vibration*, 211(5):801–818, 1998.

[9] E. Pavlovskaia and M. Wiercigroch. Modeling of an impact system with a drift. *Physical Review E - Statistical, Nonlinear, and Soft Matter Physics*, 64(5):056224: 1–9, 2001.

[10] A. Depouhon, V. Denoël, and E. Detournay. A drifting impact oscillator with periodic impulsive loading: Application to percussive drilling. *Physica D: Nonlinear Phenomena*, 258:1–10, 2013.

[11] E. V. Karpenko, M. Wiercigroch, and M. P. Cartmell. Regular and chaotic dynamics of a discontinuously nonlinear rotor system. *Chaos, Solitons and Fractals*, 13(6):1231–1242, 2002.

[12] J. Páez Chávez and M. Wiercigroch. Bifurcation analysis of periodic orbits of a non-smooth jeffcott rotor model. *Communications in Nonlinear Science and Numerical Simulation*, 18(9):2571–2580, 2013.

[13] A. Kahraman and R. Singh. Non-linear dynamics of a spur gear pair. *Journal of Sound and Vibration*, 142(1):49–75, 1990.

[14] M. R. Skeem, M. B. Friedman, B. H. Walker, et al. Drillstring dynamics during jar operation. *Journal of Petroleum Technology*, 31(11):1–381, 1979.

[15] M. Wiercigroch. Resonance enhanced drilling: method and apparatus, June 2013. US Patent 8,453,761.

[16] E. Pavlovskaia, D. C. Hendry, and M. Wiercigroch. Modelling of high frequency vibro-impact drilling. *International Journal of Mechanical Sciences*, 91:110–119, 2015.

[17] Tomax anti stick-slip technology. `https://tomax.no/`. Accessed: 2022.

[18] C. Carpenter. Faster rate of penetration in hard chalk: Proving a new hypothesis for drilling dynamics. *Journal of Petroleum Technology*, 68:59–60, 2016.

[19] T. Vromen, E. Detournay, H. Nijmeijer, and N. Van De Wouw. Dynamics of drilling systems with an antistall tool: Effect on rate of penetration and mechanical specific energy. *SPE Journal*, 24(5):194487, 2019.

[20] M. Kapitaniak, V. V. Hamaneh, and M. Wiercigroch. Torsional vibrations of helically buckled drill-strings: experiments and FE modelling. *Journal of Physics Conference Series*, 721(1):012012, 2016.

[21] Y. A. Khulief and H. Al-Naser. Finite element dynamic analysis of drillstrings. *Finite Elements in Analysis and Design*, 41(13):1270 – 1288, 2005.

[22] L. S. Hugo and M. A. Trindade. Performance analysis of proportional-integral feedback control for the reduction of stick-slip-induced torsional vibrations in oil well drillstrings. *Journal of Sound and Vibration*, 398:28 – 38, 2017.

[23] A. Chevallier, N. Politis, M. Payne, and P. Spanos. Oil and gas well drililng a vibrations perspective. *Shock Vub Dig*, 35:85–103, 2003.

[24] M. Wiercigroch. A note on the switch function for the stick-slip phenomenon. *Journal of Sound and Vibration*, 175:700–704, 1994.

[25] L. Yonggang, L. Fangpo, X. Xin, Y. Biyu, and L. Caihong. Simulation technology in failure analysis of drill pipe. *Procedia Engineering*, 12:236 – 241, 2011.

[26] S. Moradi and K. Ranjbar. Experimental and computational failure analysis of drillstrings. *Engineering Failure Analysis*, 16(3):923 – 933, 2009.

[27] E. M. Navarro-López and D. Cortés. Sliding-mode control of a multi-dof oilwell drillstring with stick-slip oscillations. In *American Control Conference*, pages 3837–3842. IEEE, 2007.

[28] E. M. Navarro-López and D. Cortés. Avoiding harmful oscillations in a drillstring through dynamical analysis. *Journal of Sound and Vibration*, 307(1):152 – 171, 2007.

[29] J. D. Jansen and L. van den Steen. Active damping of self-excited torsional vibrations in oil well drillstrings. *Journal of Sound and Vibration*, 179(4):647 – 668, 1995.

[30] A. S. Yigit and A. P. Christoforou. Coupled torsional and bending vibrations of drillstrings subject to impact with friction. *Journal of Sound and Vibration*, 215(1):167 – 181, 1998.

[31] A. P. Christoforou and A. S. Yigit. Fully coupled vibrations of actively controlled drillstrings. *Journal of Sound and Vibration*, 267:1029–1045, 2003.

[32] R. Tucker and C. Wang. On the effective control of torsional vibrations in drilling systems. *Journal of Sound and Vibration*, 224(1):101 – 122, 1999.

[33] D. R. Pavone and J. P. Desplans. Application of high sampling rate downhole measurements for analysis and cure of stick-slip in drilling. *Society of Petroleum Engineers*, 28324, 1994.

[34] J. F. Brett. The genesis of bit-induced torsional drillstring vibrations. *SPE Drilling Engineering*, 7(03):168–174, 1992.

[35] V. A. Dunayevsky and F. Abbassian. Application of stability approach to bit dynamics. *SPE Drilling and Completion*, 13(02):99–107, 1998.

[36] R. Stribeck. The key qualities of sliding and roller bearings. *Zeitschrift des Vereines Seutscher Ingenieure*, 46(38):1342–1348, 1902.

[37] J. S. Courtney-Pratt and E. Eisner. The effect of a tangential force on the contact of metallic bodies. *Proceedings of the Royal Society of London. Series A. Mathematical and Physical Sciences*, 238(1215):529–550, 1957.

[38] J. W. Liang and B. F. Feeny. Dynamical friction behavior in a forced oscillator with a compliant contact. *Journal of Applied Mechanics*, pages 627–654, 1998.

[39] J. Powell and M. Wiercigroch. Influence of non-reversible coulomb characteristics on the response of a harmonically excited linear oscillator. *Machine vibration*, 1(2):94–104, 1992.

[40] M. Wiercigroch, V. W. T. Sin, and Z. F. K. Liew. Non-reversible dry friction oscillator: design and measurements. *Proceedings of the Institution of Mechanical Engineers, Part C: Journal of Mechanical Engineering Science*, 213(5):527–534, 1999.

[41] T. M. Warren. Factors affecting torque for a roller cone bit. *Journal of Petroleum Technology*, 36-10, 1984.

[42] P. D. Spanos, A. K. Sengupta, R. A. Cunningham, and P. R. Paslay. Modeling of roller cone bit lift-off dynamics in rotary drilling. *Journal of Energy Resources Technology*, 117(3):197–207, 1995.

[43] E. Detournay and P. Defourny. A phenomenological model for the drilling action of drag bits. *International Journal of Rock Mechanics and Mining Sciences and Geomechanics Abstracts*, 29(1):13 – 23, 1992.

[44] R. Feenstra. Status of polycrystalline-diamond-compact bits: Part 1 - development. *Journal of Petroleum Technology*, 40:6, 1988.

[45] R. Feenstra. Status of polycrystalline-diamond-compact bits: Part 2 - applications. *Journal of Petroleum Technology*, 40:7, 1988.

[46] S. Dwars. Recent advances in soft torque rotary systems. *Society of Petroleum Engineers*, 173037, 2015.

[47] A. Kyllingstad and P. Nessjøen. A new stick-slip prevention system. *Society of Petroleum Engineers*, 119660, 2009.

[48] R. Wildemans, A. Aribowo, E. Detournay, and N. Van de Wouw. Modelling and dynamic analysis of an anti-stall tool in a drilling system including spatial friction. *Nonlinear Dynamics*, 98(4):2631–2650, 2019.

[49] F. Van De Velde and P. De Baets. A new approach of stick-slip based on quasi-harmonic tangential oscillations. *Wear*, 216(1):15–26, 1998.

[50] J. D. Byerlee. The mechanics of stick-slip. *Tectonophysics*, 9(5):475–486, 1970.

[51] A. Udías. Source mechanism of earthquakes. *Advances in Geophysics*, 33:81–140, 1991.

[52] D. M. Rowson. An analysis of stick-slip motion. *Wear*, 31(2):213–218, 1975.

[53] J. H. Chin and C. C. Chen. A study of stick-slip motion and its influence on the cutting process. *International Journal of Mechanical Sciences*, 35(5):353–370, 1993.

[54] V. I. Johannes, M. A. Green, and C. A. Brockley. The role of the rate of application of the tangential force in determining the static friction coefficient. *Wear*, 24(3):381 – 385, 1973.

[55] A. Harnoy, B. Friedland, and H. Rachoor. Modeling and simulation of elastic and friction forces in lubricated bearings for precise motion control. *Wear*, 172(2):155 – 165, 1994.

[56] Y. Liu, M. Wiercigroch, J. Ing, and E. Pavlovskaia. Intermittent control of coexisting attractors. *Philosophical Transactions of the Royal Society A: Mathematical, Physical and Engineering Sciences*, 371(1993):20120428, 2013.